Standardization of the Important Test Parameters in the Solder Ball Shear Test for Evaluation of the Mechanical Joint Strength

J. W. Kim, J. M. Koo, W. B. Lee, W. C. Moon, J. H. Moon, Y. M. Yeon, C. C. Shur, and S. B. Jung

Abstract

The ball shear test was investigated in terms of the effects of test parameters, i.e., shear height and shear speed, with an experimental and non-linear finite element analysis for evaluating the solder joint integrity of area array packages. Two representative Pb-free solder compositions were examined in this work: Sn-3.5Ag-0.75Cu and In-48Sn. The substrate was a common SMD type with solder bond pad openings of 460 ㎛ in diameter. The microstructural investigations were carried out using SEM, and the IMCs were identified with EDS. Shear tests were conducted with the two varying test parameters. It could be observed that increasing shear height, at fixed shear speed, has the effect of decreasing shear force for both Sn-3.5Ag-0.75Cu and In-48Sn solder joints, while the shear force increased with increasing shear speed at fixed shear height. Too high shear height could cause some undesirable effects on the test results such as unexpected high standard deviation values or shear tip sliding from the solder ball. The low shear height conditions were favorable for screening the type of brittle interfacial fractures or the degraded layers in the interfaces. The shear speed conditions were discussed with the stress analyses of the solder ball, and we cannot find any conspicuous finding which is related to optimum shear speed from the stress analyses.

Key Words : Standardization, Shear height, Shear speed, Finite element analysis, Pb-free solder, Ball grid array.

1. Introduction

Important trends in developing semiconductor devices are the small volume of products using integrated circuits (ICs) and larger size and functionality per unit area of modules used in the products. To facilitate these trends, many types of area array packages, e.g., ball grid array (BGA), chip size package (CSP) and flip chip on board (FCOB), were developed. These types of packages have evolved as a viable solution to the requirement of the industry by having matrix-arrayed solder ball terminals1). As the number of I/O pads on arrayed board increased and the size of solder joint decreased, i.e., the package density increased, the solder joint reliability has become more critical issue. Therefore, recent years have witnessed a large amount of researches concerning the properties of fine solder joints2,3). However, most of these studies are concerned primarily with discussions of the mechanical properties or the interfacial reactions between the solder and metallization of the substrate. The researches on the test methods for the mechanical strength of the solder joints or the fracture mechanisms of the joints using lead free solders were very rarely discussed, though there should be an emergent need to study the affordable test methods for package quality and reliability.

Currently, the most popular method to evaluate the strength of the solder ball attachment is the ball shear test. Although this test is simple and convenient to implement, the details of performing the test have not

J. W. Kim, J. M. Koo, W. B. Lee, W. C. Moon, J. H. Moon, C. C. Shur, and *S. B Jung* : Department of Advanced Materials Engineering, Sungkyunkwan University, Suwon, Korea
E-mail : sbjung@skku.ac.kr
Y. M. Yeon : Suwon Science College, Hwasung, Gyeonggi-do, Korea

yet been standardized for the ball shear test[4-6]. The JEDEC (Joint Electronic Devices Engineering Council) BGA ball shear standard (JESD22-B117), published in July 2000, prescribed that the gap between the edge of the shear ram and the surface of substrate should be larger than 0.05 mm and smaller than 25% of the ball height[7]. However, this specification is published in terms of a generic procedure based on the case of common 1.27 mm pitch BGA package, so cannot be applied with more fine pitch and small solder ball attachment. In addition, another important ball shear test parameter, shear speed, is not fixed in the standard. The lack of the specification in the shear speed may cause confusion in the comparison of the solder ball shear strengths characterized with different displacement rates.

Fig. 1 shows the diagrams indicating the employing frequencies of the two shear parameters in previously published research papers. These data which were published within recent 8 years of time were obtained from the web library such as IEEE and Science Direct, etc. The references on these data which were listed after the main text were summarized from about 200 full searched papers[4-6, 8-49]. These figures showed that the shear parameters were very randomly selected and displayed. This tendency is mainly due to the lack of the specification for the ball shear test, and thus the careful examination on the effect of the shear parameters should be carried out.

A significant addition to the JESD22-B117 is the incorporation of the ball shear failure mode into the acceptance criteria. The primary impetus for including failure mode is to provide a mean for screening the type of brittle interfacial fractures caused by too thick intermetallic compound (IMC) layers. During soldering, the solder alloy melts and then reacts with the metallization of the substrate to form IMCs at the joining interface[31,32]. While forming a thin IMC layer, it is desirable to achieve a good metallurgical bond. However, excessively thick reaction layer is very sensitive to stress and provides sites of initiation and paths of propagation for cracks, because the layer is brittle and a microstructural mismatch exists between the solder and pad metallization. However, during BGA ball shear test, the side-walls of the SMD (Solder Mask Defined) area array bond pads tend to support the solder joint, which can alter the failure mode. Therefore, there is a reluctance to embrace the shear technique for monitoring susceptibility to brittle interfacial failures.

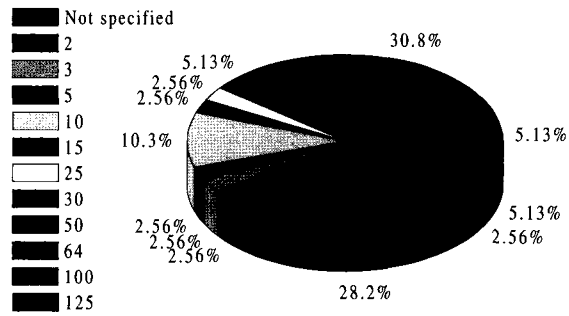

(a) shear height

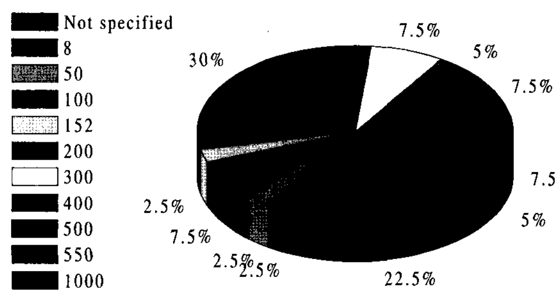

(b) shear speed

Fig. 1 Shear conditions employed in previous publications

The objectives of this study are the evaluation of the effect of important shear test parameters, such as shear height and shear speed. The recommendations for getting favorable test results and methods for finding optimum test conditions are intensively discussed. Two kinds of representative lead free solder, Sn-3.5Ag-0.75Cu and In-48Sn solders were used to observe the effects. Both experimental investigation and non-linear finite element analysis using elastic-viscoplastic constitutive model were carried out. Two finite element analysis tools, the Surface Evolver developed by Brakke and modified by Chiang and Yuan and the ANSYS were used to analyze the solder ball joints. The analytical stress and averaged equivalent plastic strain analyses were performed to interpret the failure mechanisms.

2. Experimental and FEM procedures

2.1 Experimental procedure

BGA solders used in this study were Sn-3.5Ag-0.75Cu and In-48Sn (in mass %). Solder balls of these materials had a diameter of 500 ㎛. The substrate was a SMD type bismaleimide triazine (BT) laminate with subsurface solder bond pads whose nominal size and shape were defined through a circular opening of 460 ㎛ in diameter with 1 mm pitch. The pads comprised electroplated Au over Ni over an underlying Cu pad in thickness of 0.5 and 7.0 ㎛, respectively. The Sn-3.5Ag-0.75Cu and In-48Sn solder balls were bonded to the BT substrate in a reflow process employing RMA flux in an IR four zone reflow machine (RF-430-N2, Japan Pulse Laboratory Ltd. Co.) with a maximum temperature of 255℃ and 155℃ for 60 sec. To investigate the shear height effect on the fracture mode of the joints having relatively thick IMC layers, two aging conditions of 180℃ and 110℃ for 200 hours were employed. The microstructural observation was conducted with scanning electron microscope (SEM) and compositions of the resulting IMCs were measured by energy dispersive spectrometer (EDS). Shear tests were conducted using a global bond tester (Dage-4000s, Richardson Electronics Ltd.) in various test conditions. The shear test conditions of this work are given in Table 1 and Table 2. The fracture mode of each test site was examined after shear testing to evaluate the mode of failure.

Table 1 Examined shear height conditions

Shear speed (㎛/s)	Shear height (㎛)					
200	10	30	50	70	90	120

Table 2 Examined shear speed conditions

Shear height (㎛)	Shear speed (㎛/s)						
50	10	50	100	200	300	400	500

2.2 Finite element analysis

The reflow geometry of the solder ball was predicted using the Surface Evolver program. The Surface Evolver is an energy-based method for predicting the shape of a liquid body. To simulate the geometric shape of a liquid body, the Surface Evolver deconstructs the initial simplex surface of a liquid body into a set of triangular facets and then iterates these facets toward a minimal energy equilibrium situation using a gradient descent method. In a situation of static equilibrium, the total energy of a liquid body is generally comprised of three major energy portions, i.e., surface tension energy, gravitational energy, and external energy related to body volume change. Fig. 2 shows the general cross-sectional view of a reflowed Sn-3.5Ag-0.75Cu solder joint and the 3-dimensional (3-D) finite element model predicted by the Surface Evolver. To confirm the accuracy of geometric prediction, actual measurements of solder balls were compared to the prediction. Table 3 compares the solder ball diameter, solder ball height and contact angle for the actual and predicted solder ball revealing a close agreement between the Surface Evolver prediction and the actual values.

Table 3 Comparison of solder ball shape between actual and predicted model

	Actual model	Predicted model
Solder ball diameter (㎛)	553.9[a]/538.2[b]	554.7[a]/536.9[b]
Solder ball height (㎛)	394.3[a]/408.3[b]	392.1[a]/410.2[b]
Contact angle (degree)	58.7[a]/63.2[b]	57.2[a]/62.9[b]

(Note: Sn-3.5Ag-0.75Cu[a], In-48Sn[b])

The key points of the solder ball surface were obtained from the Surface Evolver prediction using a curve fitting program, and then used to construct the solder ball model in ANSYS software. For analysis time saving, 2-D elastic-viscoplastic finite element simulation methodologies were utilized to predict the

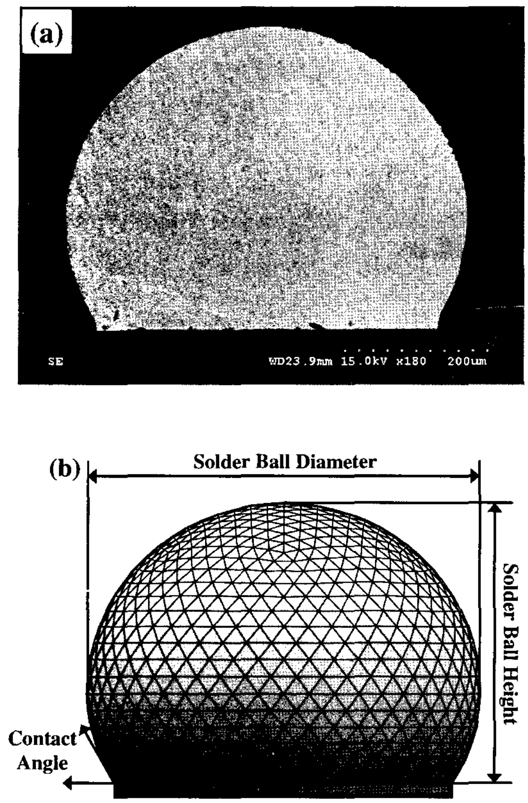

Fig. 2 Geometric profile comparison between actual (a) and predicted solder ball attachment (b).

effect of ball shear parameters on shear force. The components of finite element simulation included a reflowed solder ball, the BT substrate, the subsurface Cu pad, and the electroplated Ni layer. The shear ram was considered as a rigid body. The surface-to-surface target element (TARGE169) and the contact element (CONTA172) were employed to simulate the contact between the shear ram and the solder ball. Figs. 3 (a) and (b) show the overall 2-D finite element model for the Sn-3.5Ag-0.75Cu solder ball shear test and the magnified view near the left side of the Ni layer, respectively.

Because the test temperature was in excess of a homologous temperature of 0.5, linear and non-linear, time dependent and independent material properties were incorporated in the finite element model. In the present work, the generalized Garofalo creep model for Sn-3.5Ag-0.75Cu solder and the power-law creep model for In-48Sn solder were employed to represent the viscoplastic behavior of solder. These models have been widely used to characterize the solder's inelastic, time-dependent behavior. The detailed description of the models could be found in our previous researches[37,48]. The creep option was combined with Multilinear Isotropic (MISO) hardening using von Mises plasticity to represent the viscoplastic properties of the solder material.

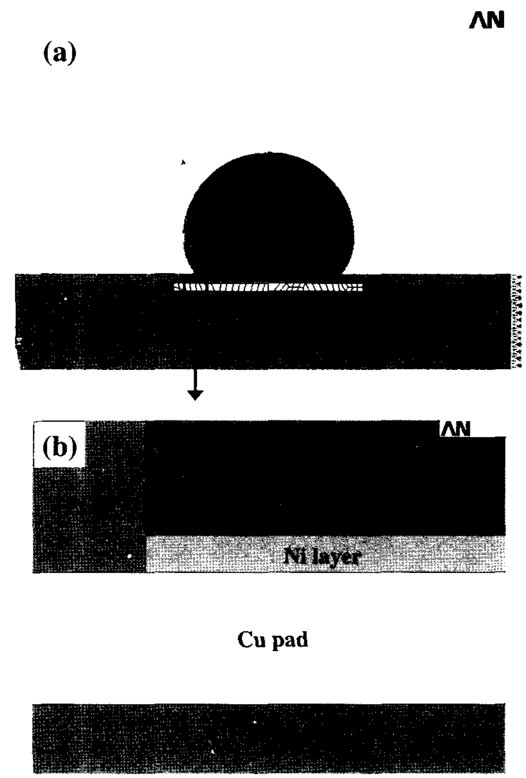

Fig. 3 Finite element model for the ball shear test (a) and magnified view near the Ni layer (b)

3. Results and discussion

3.1 Verification of the FEM results

The averaged incremental equivalent plastic strain analysis was performed to determine the failure mode of the shear tested solder joints, because the load on the pad site of the solder ball during a shear test is a mixture of tensile, shear and compressive forces, especially at the corners of the solder. Figs. 5 (a) and

(b) plot the distributions of the averaged equivalent plastic strain for the base case, shear height of 50 μm and shear speed of 200 $\mu m/s$, of the Sn-3.5Ag-0.75Cu and In-48Sn joints, respectively. From Fig. 4, the high plastic strain region in the solder ball is near the contact point between the shear ram and the solder, and had expanded through the solder in parallel to the substrate. This implies a strong likelihood of crack initiation and growth through this region. The cross-sectional views of the solder balls after the shear testing are shown in Fig. 5. Comparing Fig. 4 with Fig. 5, the shear failure modes of solder ball joints, determined by computational analysis, well correlate with the actual solder ball failure modes under the shear test.

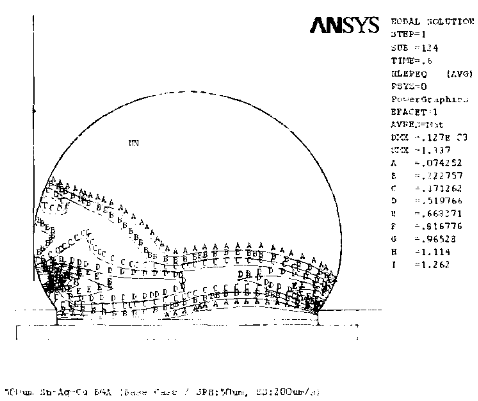

(a) Sn-3.5Ag-0.75Cu

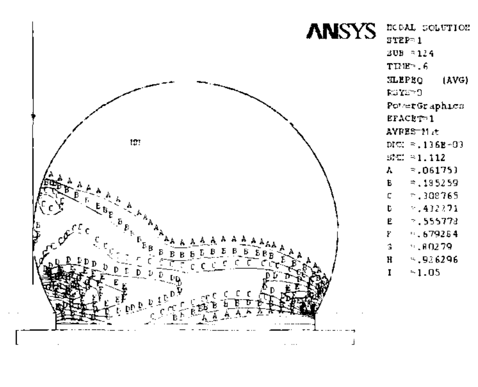

(b) In-48Sn

Fig. 4 Contour plots of averaged equivalent plastic strain analysis in the base case condition (shear height: 50 μm, shear speed: 200 $\mu m/s$)

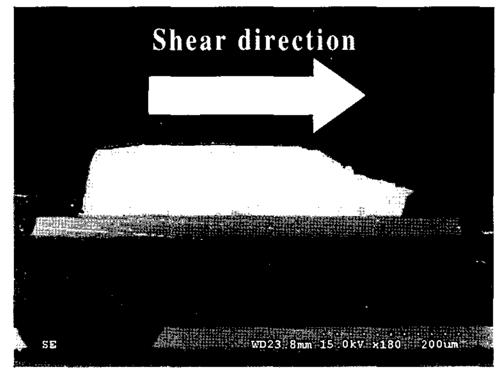

(a) Sn-3.5Ag-0.75Cu

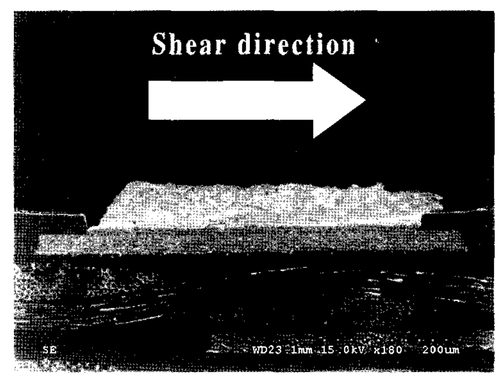

(b) In-48Sn

Fig. 5 Cross-sectional views after ball shear test in the base case condition (shear height: 50 μm, shear speed: 200 $\mu m/s$)

Figs. 6 (a) and (b) show the force-displacement curves from the experiment and modeling computations at the base condition, corresponding to Sn-3.5Ag-0.75Cu and In-48Sn solder, respectively. The maximum shear force of the Sn-3.5Ag-0.75Cu solder joint is higher than that of In-48Sn solder joint, and this is consistent with the results from the previous studies[37,48]. The difference of the shear force between the two solders is mainly considered to be due to the extreme softness of the indium material. The graphs from the experiment and modeling show similar concave down behavior except for the first stage of curves where the experimental curves show a concave up region which seems to be mainly due to the experimental errors such as flux residues. Alternately, the reflowed ball shape may produce a concave up Hertzian loading curve characteristic of increasing contact area with the ram of the shear tester. From the two results mentioned above, it could be concluded that the finite element analysis used in this study is sufficiently reliable.

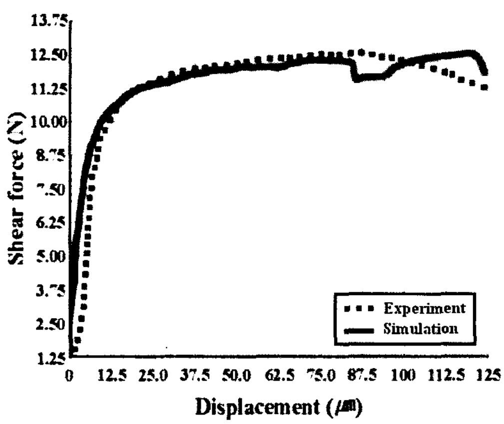

(a) Sn-3.5Ag-0.75Cu

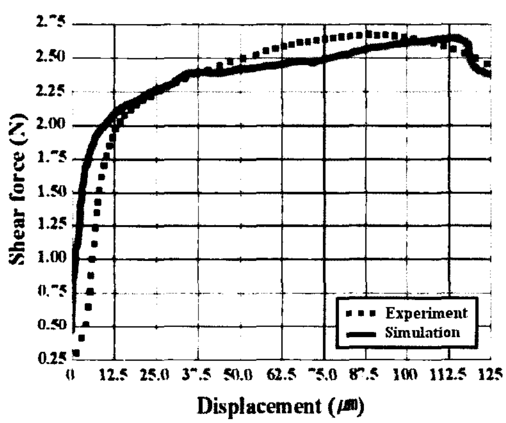

(b) In-48Sn

Fig. 6 Force-displacement curves in the base case condition (shear height: 50 ㎛, shear speed: 200 ㎛/s)

3.2 Microstructures of the solder joints

Figs. 7 (a) and (b) show back scattered electron (BSE) micrographs of the interfaces between the two kinds of solders and the Au/Ni electroplated layer on the Cu pad. In case of the Sn-3.5Ag-0.75Cu solder joints, a continuous layer of $(Ni_{1-x}Cu_x)_3Sn_4$ and a discontinuous $(Cu_{1-y}Ni_y)_6Sn_5$ particles could be seen, while the Au layer appears to have dissolved into the liquid solder leaving no observable Au at the interface as shown in Fig. 7 (a). The compositions of these phases, determined by EDS, were $(Ni_{0.72}Cu_{0.28})_3Sn_4$ and $(Cu_{0.66}Ni_{0.34})_6Sn_5$, respectively. Some Ag_3Sn IMCs were distributed inside the Sn-3.5Ag-0.75Cu solder, and could be considered as an influential factor controlling the mechanical properties of the solders[37].

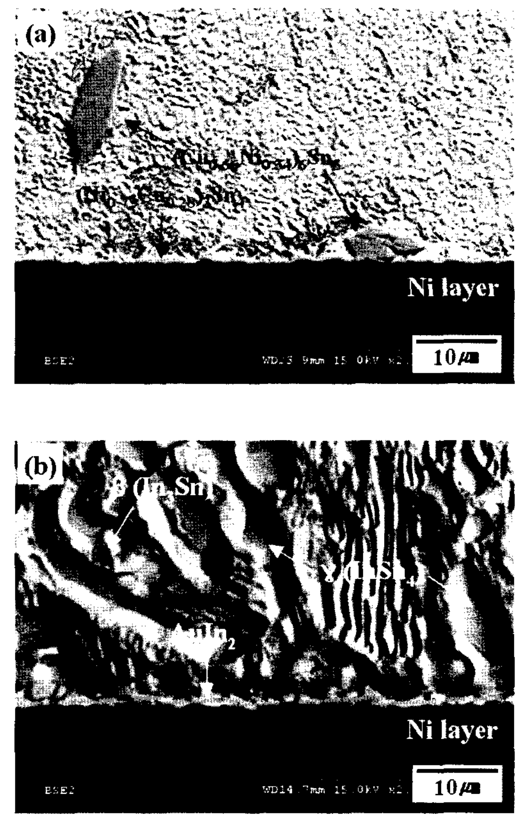

Fig. 7 SEM micrographs of Sn-3.5Ag-0.75Cu (a), and In-48Sn (b) solder joint interface

In case of the In-48Sn solder joints, as shown in Fig. 7 (b), the microstructure of the solder which consists of two intermetallic phases, i.e., In-rich β and Sn-rich γ phase, shows a general lamellar structure with fan-shaped eutectic colonies. From the literatures, the β phases were known to be pseudo-body-centered tetragonal structure while the γ phases were hexagonal phases. Based on the EPMA analysis, the compositions of the two phases could be analyzed to be In3Sn and InSn4, respectively[48]. This microstructure could be also considered as an influential factor controlling the mechanical properties of the solder, and these considerations were assumed to be properly applied with the power law constitutive model and MISO hardening model. At the interface between the In-48Sn and substrate, a layer of Au-In IMC was formed in thickness of about 1.5 ㎛, while Au layer also appears to have reacted with the solder leaving no observable Au at the interface. From the EPMA analyses, the Au-In IMC was observed to be indicating AuIn2 phase. Too thick interfacial IMC layer is sensitive to stress and provides sites of initiation and paths of propagation for cracks, because the layer is brittle and a microstructural mismatch exists between solder and metallization. Therefore, the growth of IMC layer could degrade the solder ball shear strength. For this reason, from the electronic package reliability point of view, it is very important to screen the brittle interfacial fracture or to identify weak interfaces in solder joints when high temperature storage, burn-in, or extended bake-out creates thick IMC layers[49].

3.3 Analysis of shear height

Figs. 8 (a) and (b) show the shear force variations of experiment and computational modeling under increasing shear height, corresponding to Sn-3.5Ag-0.75Cu and In-48Sn, respectively. Experimentally, for each test condition, 30 solder balls were sheared to failure. The shear force decreased with increasing shear height and reached the minimum value at the highest height. This means that the resistance to plastic deformation is increased by increasing contact area between the shear ram and bulk solder. In the same manner, the computational results indicate that the shear force decreased with increasing shear height. The phenomenological situation and the mathematical calculation are in qualitative agreement, supporting the logic that the decrease in shear force with increasing shear height is a direct consequence of the material properties of the package components and the geometrical shape of the solder ball. However, it should be also noted that, in the cases of higher shear height than 50 ㎛ for the Sn-3.5Ag-0.75Cu and 70 ㎛ for the In-48Sn, both the mismatches between the experimental and computational results and standard deviation values from the experimental results increased. These were because the contact area between the shear ram and solder was so confined, while the local deformation in the solder had become too severe (the edge of shear ram cuts deep into the solder ball due to high ram height). In addition, the shear probe sliding from the solder ball was frequently occurred in the high shear height test conditions, especially 90 and 120 ㎛ of shear height. Consequently, in the high shear probe height, the shear force results from the experiment could be more susceptible to the experimental factors such as indefinite quantity of the solder applied to the pad resulting in different ball shape, flux residues on ball surface, compliance of the shear test fixturing and oxidation at the BGA surface, etc. From the engineering point of view, too high shear height should be kept away from the test conditions.

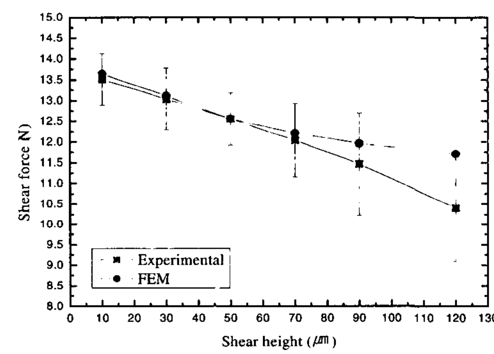

(a) Sn-3.5Ag-0.75Cu

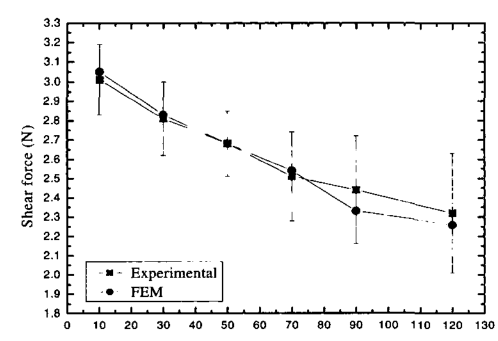

(b) In-48Sn

Fig. 8 Shear force variations with increasing shear height

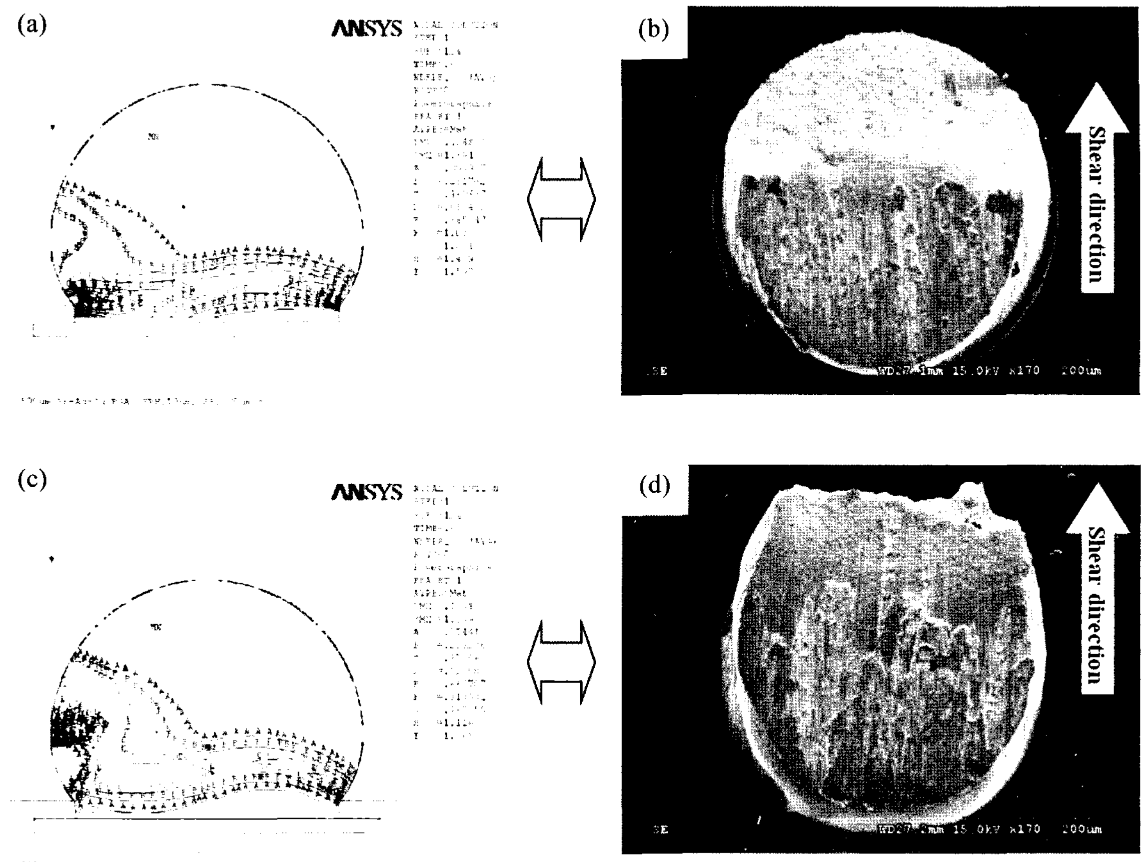

Fig. 9 Distributions of averaged equivalent plastic strain and fracture surfaces after shear test of Sn-3.5Ag-0.75Cu solder joints; (a), (b) 10 μm of shear height and (c), (d) 120 μm of shear height

Fig. 9 shows the distributions of averaged equivalent plastic strain and the fracture surfaces of the test specimens after shear testing of Sn-3.5Ag-0.75Cu solder joints. Figs. 9 (a) and (b) are the cases of 10 μm shear height with 200 μm/s shear speed, and Figs. 9 (c) and (d) are the cases of 120 μm shear height with 200 μm/s shear speed. As shown in the figures, the strain is very densely accumulated in the right above the Ni layer for the case of 10 μm shear height, while the strain is spread out in the upper region of the solder for the case of 120 μm shear height. This is well correlated with the corresponding fracture surfaces shown in Figs. 9 (b) and (d). Furthermore, the maximum value of strain in the Fig. 9 (a) is higher than that of Fig. 9 (c). Therefore, it could be deduced that, if the IMC layer between the solder and pad metallization is sufficiently thick, the brittle interfacial failure could be more easily achieved for the cases of lower shear height.

Fig. 10 presents the von Mises stress distributions within the Cu pad and Ni layer. The figure indicates that the application of shear loads to a multi-phase structure results in the formation of a singularity phenomenon, i.e., a stress concentration, at the corner of the common boundary of two different materials. This is due to the phase discontinuity which occurs at this boundary. However, the location of the maximum stress is different between two cases, shear height of 10 μm and 120 μm. The maximum stress region is located in the left corner of the Ni layer when the shear height is 10 μm, while the stress is concentrated in the right corner of the Ni layer that could not be the initiation of the failure path when the shear height is 120 μm. This means that the cases with lower shear height could screen the type of brittle interfacial fractures or the degraded layers in the interfaces more easily. Even though the maximum stress occurs within the Ni layer,

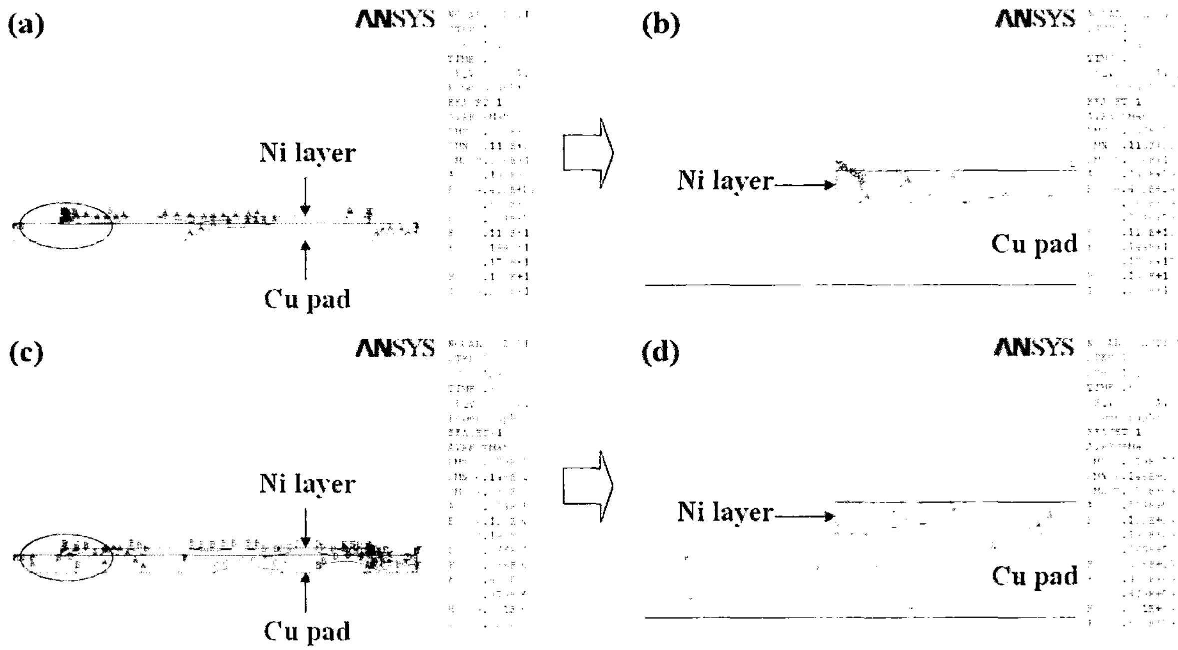

Fig. 10 Von Mises stress contours within the Cu pad and Ni layer; (a), (b) 10 μm of shear height, (c), (d) 120 μm of shear height.

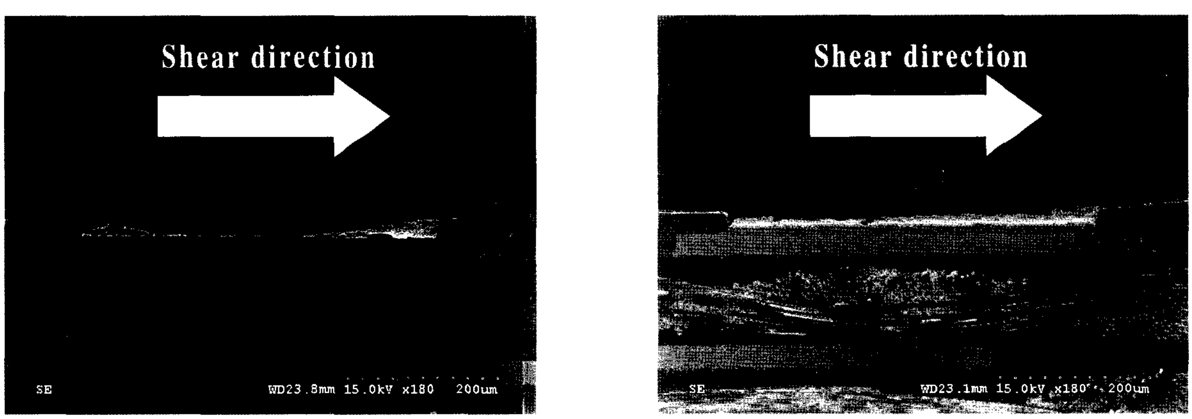

(a) Sn-3.5Ag-0.75Cu (b) In-48Sn

Fig. 11 General cross-sectional view after shear test of the aged specimen in the condition of 10 μm shear height

cracking does not readily occur near this layer since the strengths of the IMCs or Ni are greater than the strength of the solder. Accordingly, it could be said that when the thickness of the interfacial IMC layer is thicker, the brittle interfacial failure could be achieved for the cases of lower shear height.

Fig. 11 shows the general cross-sectional views of the aged Sn-3.5Ag-0.75Cu and In-48Sn solder joints after shear testing in the condition of 10 μm shear height with 200 μm/s shear speed. The aging condition for the sample in Fig. 11 (a) is 180℃ temperature with 200 hours aging time, while for the sample in Fig. 11 (b) is 110℃ temperature with 200 hours aging time. As shown in the figures, the failure type was a mixed mode of ductile and brittle. About 70% of the Sn-3.5Ag-0.75Cu and 90% of the In-48Sn solder joints

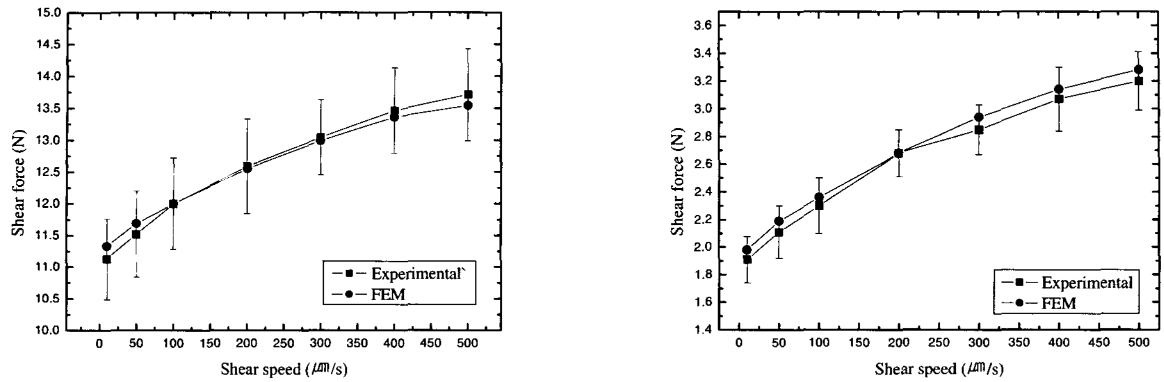

(a) Sn-3.5Ag-0.75Cu (b) In-48Sn

Fig. 12 Shear force variations with increasing shear speed

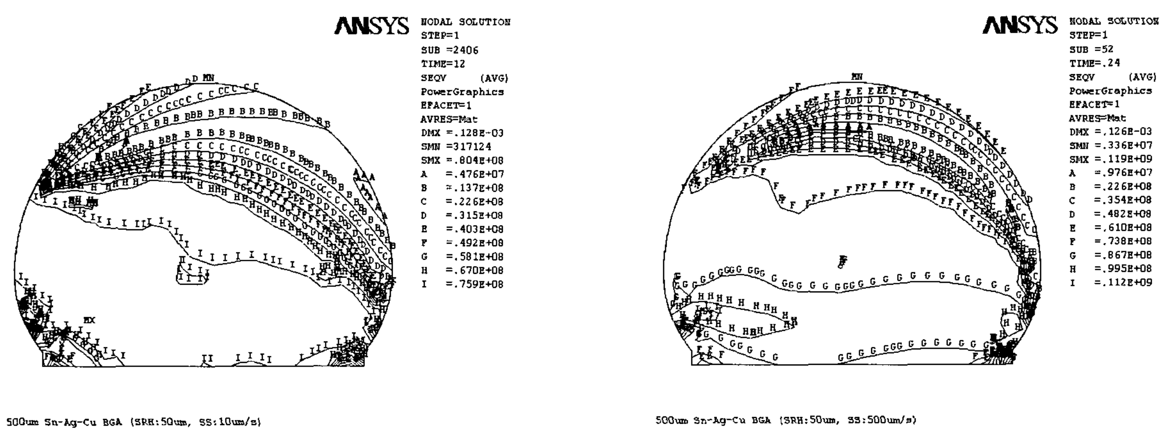

(a) 10 ㎛/s of shear speed (b) 500 ㎛/s of shear speed

Fig. 13 Von Mises stress contours within the Sn-3.5Ag-0.75Cu solder

exhibited this mixed mode of failure or brittle failure mode, while very limited number of the specimens resulted in mixed failure mode in other test conditions. This is very well agreed with the simulation results described in the above.

3.4 Analysis of shear speed

The shear force variations of experiment and computational modeling under increasing shear speed are shown in Fig. 12. The shear force is proportional to the shear speed and reaches a maximum value at the highest shear speed in both the experimental and computational results. This means that the increase in shear force with increasing shear speed is a direct consequence of the material properties including both time-independent plastic hardening and time-dependent creep. According to Nadai's mathematical analysis, a general relationship between flow stress and strain rate, at constant strain and temperature, can be expressed by[50]

$$\sigma = C\left(\frac{d\varepsilon}{dt}\right)^{s}\Big|_{\varepsilon,T}$$

where s is known as the strain-rate sensitivity and C is a constant. The exponent s can be obtained from the slope of a plot of $\log\sigma$ vs. $\log(d\varepsilon/dt)$. In ordinary metals having high melting point, the strain-rate sensitivity (s) is quite low (< 0.1) at room temperature, but s increases with temperature, especially at temperatures above a homologous temperature of 0.5. Because the room temperature is higher than half of the melting point of solders in absolute temperature, the strain rate or displacement rate is very important to the stress flow properties. According to this study, shear force of low melting point In-48Sn solder increased from about 1.9 to 3.2 N with the shear speed ranged from 10 to 500 ㎛/s, i.e., about 70% rise of the shear force. This is well explaining the theory mentioned above.

Fig. 13 shows the von Mises stress contour analyses of the Sn-3.5Ag-0.75Cu for the two test conditions which were shear speed of 10 ㎛/s and 500 ㎛/s with fixed shear height of 50 ㎛. The highest stress region of the mere solder ball was covering the fracture locations which were shown in Figs. 5 and 9. This means that the ball shear mode is also closely related to the high region of von Mises stress contours. In the figure, the von Mises stress values increased with increasing shear speed, giving rise to the increasing ball shear forces as reported in Fig. 12. However, we cannot find out the effect of shear speed on the variation of the failure mode in the shear tested solder ball joints. Therefore, we could not find any optimum shear speed condition in the shear test of the BGA/CSP solder joints. However, the statement of the shear test conditions on someone's experimental reports should be specified in their publications.

4. Conclusion

The analyses of the test method for the strength of BGA solder joints were carried out. The results are used to draw following conclusions.

1. The reflowed solder ball shape was successfully predicted by the energy-based simulation tool, i.e., Surface Evolver. The results from the simulation using ANSYS, such as the averaged equivalent plastic strain and the force-displacement curves, indicated that the finite element analysis used in this study was reasonably reliable.

2. The continuous layer of $(Ni_{0.72}Cu_{0.28})_3Sn_4$ and some IMC particles of $(Cu_{0.66}Ni_{0.34})_6Sn_5$ were found between the pad and Sn-3.5Ag-0.75Cu solder, while only $AuIn_2$ IMC layer was formed at the interface between the Au/Ni layer on Cu pad and In-48Sn solder in thickness of about 1.5 ㎛.

3. It could be observed that increasing shear height, at fixed shear speed, has the effect of decreasing shear force in both experimental and computational results. These were considered to be due to the decreasing contact area between the shear ram and bulk solder.

4. Too high shear height could cause some undesirable effects on the test results, e.g., unexpected high standard deviation values or shear tip sliding from the solder ball surface. Therefore, the shear test conditions with exceeding shear height of 15% of the solder ball height should be avoided.

5. From the computational results, the relatively low shear height conditions were favorable for screening the type of brittle interfacial fractures or the degraded layer in the interfaces. This was well matched to the experimental results performed with the aged samples.

6. The shear force increased with increasing shear speed at fixed shear height of 50 ㎛. The shear force of the Sn-3.5Ag-0.75Cu solder joints increased about 30%, while the shear force of the low melting point In-48Sn solder joints increased about 90% with increasing shear speed from 10 to 500 ㎛. It should be noted that the sensitivity of shear speed in In-48Sn solder is largely higher than those of Sn-based solders.

7. The choice of the shear speed for someone's shear test should be carefully conducted with the considerations of the effects of solder material properties such as the viscoplasticity or creep. Because of these properties, the effect of the shear speed on the shear force of the joints should be very high, and thus the selected condition should be specified in someone's research reports.

Acknowledgements

The present work was carried out with the support of a 'Municipal Leading Support Program for Research and Development (Project No. 2004-0693-100)' of the Korea Ministry of Commerce, Industry and Energy accompanying with the Gyeonggi Province. The financial support from the Korea Ministry of Commerce, Industry and Energy under the Standardization-Technology-Development-Program (Project No. 10012693) is also gratefully acknowledged.

References

1. W. J. Choi, E. C. Yeh, and K. N. Tu : Mean-time-to-failure study of flip chip solder joints on Cu/Ni(V)/Al thin-film under-bump-metallization, *Journal of Applied Physics*, Vol. 94, No. 9 (2003), pp. 5665-5671
2. D. G. Kim, J. W. Kim, J. G. Lee, H. Mori, D. J. Quesnel, and S. B. Jung : Solid state interfacial reaction and joint strength of Sn-37Pb solder with Ni-P under bump metallization in flip chip application, *Journal of Alloys and Compounds*, (IN-PRESS)
3. J. W. Jang, L. N. Ramanathan, J. K. Lin, and D. R. Frear : Spalling of Cu_3Sn intermetallics in high-lead 95Pb5Sn solder bumps on Cu under bump metallization during solid-state annealing, *Journal of Applied Physics*, Vol. 95, No. 12 (2004), pp. 8286-8289
4. J. W. Kim, J. W. Yoon, and S. B. Jung : Influence of shear speed on the shear force of eutectic Sn-Pb and Pb-free BGA solder joints, *Materials Science Forum*, Vol. 449-452, (2004), pp. 897-900
5. J. W. Kim, J. Joo, D. J. Quesnel, and S. B. Jung : Correlation between the displacement rate and shear force in the shear test of Sn-Pb and Pb-free solder joints, *Materials Science and Technology*, (IN-PRESS)
6. J. W. Kim, S. K. Park, and S. B. Jung : Analysis of the test parameters in the shear test of BGA solder joints, *Key Engineering Materials*, (IN-PRESS)
7. JESD22-B117, *JEDEC Solid State Technology Association*, (2000)
8. X. Huang, S. W. R. Lee, and C. C. Yan : Experimental investigation on the progressive failure mechanism of solder balls during ball shear test, *Electronic Components and Technology Conference*, (2002), pp. 28-31
9. H. T. Lee, T. L. Liao, and M. H. Chen : Study on microstructure and shear strength of Sn-Ag-Sb solder joints, *Electronic Materials and Packaging Conference*, (2001), pp. 315-322
10. M. S. Shin and Y. H. Kim : Intermetallic formation in the Sn-Ag solder joints between Au stud bumps and Cu pads and its effect on the chip shear strength, *Electronic Materials and Packaging Conference*, (2001), pp. 155-162
11. A. Syed : Reliability and Au embrittlement of lead free solders for BGA applications, *Advanced Packaging Materials Conference*, (2001), pp. 143-147
12. J. W. Choi and T. S. Oh : Shear strength and aging characteristics of Sn-Pb and Sn-Ag-Bi solder bumps, *Electronic Materials and Packaging Conference*, (2001), pp. 433-437
13. X. Huang, S. W. R. Lee, C. C. Yan, and S. Hui : Characterization and analysis on the solder ball shear testing conditions, *Electronic Components and Technology Conference*, (2001), pp. 1065-1071
14. L. Li, J. W. Jang, and B. Allmen : Shear property and microstructure evaluation of Pb-free solder bumps under room temperature and multiple reflow/high temperature aging, *Advanced Packaging Materials Conference*, (2001), pp. 347-353
15. N. M. Poon, C. M. L. Wu, J. K. L. Lai, and Y. C. Chan : Residual shear strength of Sn-Ag and Sn-Bi lead-free SMT joints after thermal shock, *IEEE Transactions on Advanced Packaging*, Vol. 23, No. 4, (2000), pp. 708-714
16. R. J. Coyle, P. P. Solan, A. J. Serafino, and S. A. Gahr : The influence of room temperature aging on ball shear strength and microstructure of area array solder balls, *Electronic Components & Technology Conference*, (2000), pp. 160-169
17. R. J. Coyle and P. P. Solan : The influence of test

parameters and package design features on ball shear test requirements, *Electronics Manufacturing Technology Symposium*, (2000), pp. 168-177
18. C. K. Shin and J. Y. Huh : Effect of Cu-containing solders on the critical IMC thickness for the shear strength of BGA solder joints, *Electronics Packaging Technology Conference*, (2000), pp. 406-411
19. X. Huang, S. W. R. Lee, and W. S. Tse : Experimental characterizations for the shear strength of Pb-free solder balls on a PZT substrate with Pd/Ag pads, *Electronics Packaging Technology Conference*, (2000), pp. 86-90
20. C. Jian, S. Law, A. Teng, and P. C. H. Chan : Influences of pad shape and solder microstructure on shear force of low cost flip chip bumps, *Electronic Materials and Packaging*, (2000), pp. 91-98
21. R. Erich, R. J. Coyle, G. M. Wenger, and A. Primavera : Shear testing and failure mode analysis for evaluation of BGA ball attachment, *Electronics Manufacturing Technology Symposium*, (1999), pp. 16-22
22. S. C. Hung, P. J. Zheng, S. C. Lee, and J. J. Lee : The effect of Au plating thickness of BGA substrates on ball shear strength under reliability tests, *Electronics Manufacturing Technology Symposium*, (1999), pp. 7-15
23. K. L. Lin and Y. C. Liu : Shearing strength and materials interaction during reflow of Al/Cu/electroless nickel/solder bump, *Electronic Components and Technology Conference*, (1999), pp. 607-612
24. G. J. S. Chou : Microstructure evolution of SnPb and SnAg/Cu BGA solder joints during thermal aging, *Advanced Packaging Materials Conference*, (2002), pp. 39-46
25. H. Tsunetsugu, T. Hayashi, and K. Katsura : Micro-alignment technique using 26-μm diameter microsolder bumps and its shear strength, *Electronic Manufacturing Technology Symposium*, (1996), pp. 52-55
26. R. J. Coyle, A. Holliday, P. Mescher, P. P. Solan, S. A. Gahr, H. A. Cyker, K. Dorey, and T. I. Ejim : The influence of nickel/gold surface finish on the assembly quality and long term reliability of thermally enhanced BGA packages, *Electronics Manufacturing Technology Symposium*, (1999), pp. 23-35
27. C. H. Lee, S. G. Lee, and B. H. Moon : Comparison of the shear strength and reliability between gold-plated and bare copper lands of a BGA package, *Electronic Components & Technology Conference*, (1998), pp. 1103 -1108
28. Z. Na, M. McNicholas, and N. Colvin : Microstructural and compositional failure analysis of Cr-CrCu-Cu thin films for ball grid array (BGA) applications, *Physical & Failure Analysis of Integrated Circuits Conference*, (1997), pp. 44-49
29. S. J. Cho, J. Y. Kim, M. G. Park, S. Park, and H. S. Chun : Under bump metallurgies for a wafer level CSP with eutectic Pb-Sn solder ball, *Electronic Components & Technology Conference*, (2000), pp. 844-849
30. Y. Tian, C. Wang, X. Ge, P Liu, and D. Liu : Intermetallic compounds formation at interface between PBGA solder ball and Au/Ni/Cu/BT PCB substrate after laser reflow processes, *Materials Science and Engineering B*, Vol. 95, No. 3 (2002), pp. 254-262
31. J. W. Yoon, S. W. Kim, and S. B. Jung : Effect of reflow time on interfacial reaction and shear strength of Sn-0.7Cu solder/Cu and electroless Ni-P BGA joints, *Journal of Alloys and Compounds*, Vol. 385, No. 1-2 (2004), pp. 192-198
32. J. W. Yoon, S. W. Kim, and S. B. Jung : IMC morphology, interfacial reaction and joint reliability of Pb-free Sn-Ag-Cu solder on electrolytic Ni BGA substrate, *Journal of Alloys and Compounds*, (IN-PRESS)
33. A. Sharif, M. N. Islam, and Y. C. Chan : Interfacial reactions of BGA Sn-3.5%Ag-0.5%Cu and Sn-3.5%Ag solders during high-temperature aging with Ni/Au metallization, *Materials Science and Engineering B*, Vol. 113, No. 3 (2004), pp. 184-189
34. J. W. Yoon, S. W. Kim, and S. B. Jung : Interfacial reaction and mechanical properties of eutectic Sn-0.7Cu/Ni BGA solder joints during isothermal long-term aging, *Journal of Alloys and Compounds*, (IN-PRESS)
35. K. S. Kim, K. W. Ryu, C. H. Yu, and J. M. Kim : The formation and growth of intermetallic

compounds and shear strength at Sn-Zn solder/Au-Ni-Cu interfaces, *Microelectronics Reliability*, (IN-PRESS)

36. J. Wang, H. K. Lim, H. S. Lew, W. T. Saw, and C. H. Tan : A testing method for assessing solder joint reliability of FCBGA packages, *Microelectronics Reliability*, Vol. 44, No. 5 (2004), pp. 833-840
37. J. W. Kim and S. B. Jung : Experimental and finite element analysis of the shear speed effects on the Sn-Ag and Sn-Ag-Cu BGA solder joints, *Materials Science and Engineering A*, Vol. 371, No. 1-2 (2004), pp. 267-276
38. M. N. Islam, Y. C. Chan, A. Sharif, and M. O. Alam : Comparative study of the dissolution kinetics of electrolytic Ni and electroless Ni-P by the molten Sn3.5Ag0.5Cu solder alloy, *Microelectronics Reliability*, Vol. 43, No. 12 (2003), pp. 2031-2037
39. J. Zheng, J. Z. Lee, K. H. Liu, J. D. Wu, and S. C. Hung : Solder joint reliability of TFBGA assemblies with fresh and reworked solder balls, *Microelectronics Reliability*, Vol. 43, No. 6 (2003), pp. 925-934
40. K. S. Kim, C. H. Yu, N. H. Kim, N. K. Kim, H. J. Chang, and E. G. Chang : Isothermal aging characteristics of Sn-Pb micro solder bumps, *Microelectronics Reliability*, Vol. 43, No. 5 (2003), pp. 757-763
41. Y. Tian, C. Wang, X. Ge, P. Liu, and D. Liu : Intermetallic compounds formation at interface between PBGA solder ball and Au/Ni/Cu/BT PCB substrate after laser reflow processes, *Materials Science and Engineering B*, Vol. 95, No. 3 (2002), pp. 254-262
42. M. O. Alam, Y. C. Chan, and K. C. Hung : Reliability study of the electroless Ni-P layer against solder alloy, *Microelectronics Reliability*, Vol. 42, No. 7 (2002), pp. 1065-1073
43. L. Haiying, A. Johnson, and C. P. Wong : Development of new no-flow underfill materials for both eutectic Sn-Pb solder and a high temperature melting lead-free solder, *IEEE Transactions on Components and Packaging Technologies*, Vol. 26, No. 2 (2003), pp. 466-472
44. L. Ming, K. Y. Lee, D. R. Olsen, W. T. Chen, B. T. C. Tan, and S. Mhaisalkar : Microstructure, joint strength and failure mechanisms of SnPb and Pb-free solders in BGA packages, *IEEE Transactions on Electronics Packaging Manufacturing*, Vol. 25, No. 3 (2002), pp. 185-192
45. M. Painaik, D. L. Santos, A. J. McLenaghan, P. Chouta, and S. K. Johnson : Effect of flux quantity on Sn-Pb and Pb-free BGA solder shear strength, *Electronics Manufacturing Technology Symposium*, (2002), pp. 229-237
46. C. M. T. Law and C. M. L. Wu : Microstructure evolution and shear strength of Sn-3.5Ag-RE lead-free BGA solder balls, *IEEE CPMT Conference*, (2004), pp. 60-66
47. C. M. T. Wu and C. M. L. Wu : Microstructure evolution and shear strength of eutectic Sn-9Zn and Sn-0.7Cu lead-free BGA solder balls, *IEEE CPMT Conference*, (2004), pp. 47-51
48. J. W. Kim, D. G. Kim, J. M. Koo, and S. B. Jung : Effect of shear speed on the shear force of low melting point BGA solder joints, *Electronic Materials and Packaging Conference*, (2003), pp. 282-288
49. J. W. Kim, S. K. Park, and S. B. Jung : Optimum shear height for evaluation of Pb-free solder ball shear strength, *Materials Science Forum*, Vol. 486-487, (2005), pp. 269-272
50. A. Nadai : Theory of Flow and Fracture of Solids, *McGraw-Hill, Inc.*, New York, (1950), p. 535